





Cite this: *Nanoscale*, 2019, **11**, 12619

Quantum-confined stark effect in the ensemble of phase-pure CdSe/CdS quantum dots†

Lei Zhang,^a Bihu Lv,^b Hongyu Yang,^a Ruilin Xu,^a Xiaoyong Wang,^{*b} Min Xiao,^b Yiping Cui ^a and Jiayu Zhang ^{*a}

Colloidal semiconductor quantum dots (QDs) have recently attracted great attention in electric field sensing *via* the quantum-confined Stark effect (QCSE), but they suffer from the random local electric field around the charged QDs through the Auger process or defect traps. Here, QCSE in the ensemble of phase-pure wurtzite CdSe/CdS QDs was studied by applying a uniform external electric field. We observed clear field-dependent photoluminescence (PL) and absorption characteristics in thick-shell CdSe/CdS QDs with 11 CdS monolayers (11 MLs) including a pronounced spectral redshift in PL of ~2.3 nm and absorption of ~2.1 nm. The time-dependent PL intensity traces implied that the thick-shell QDs were conducive to realize the Stark shift in QD ensembles due to the effective suppression of the main sources of the local field. These findings were in stark contrast to those of moderate-shell (5 MLs) and ultrathick-shell (15 MLs) CdSe/CdS QDs. The measurement value of exciton polarizability was smaller than the theoretical value, which may be influenced by very few exciton traps. Moreover, the amplified stimulated emission also exhibited obvious optical modulations under the electric field with decreased emission intensity and an increased ultrafast lifetime. Finally, the temporal evolution of the multiexciton process in thick-shell CdSe/CdS QDs indicated that the multiexciton state induced a higher energy state near the band edge, which may weaken the QCSE of a single exciton. Therefore, it was demonstrated that efficient field control over the optical properties of these nanomaterials is feasible and this can open up potential applications in field-controlled electro-optic modulators.

Received 9th April 2019,
Accepted 10th June 2019

DOI: 10.1039/c9nr03061a

rsc.li/nanoscale

Introduction

Colloidal semiconductor quantum dots (QDs) have composition- and size-tunable optical properties as well as the beneficial features of narrow emission peaks and high quantum yields (QYs).^{1,2} Besides, the intricate control over the shape, heterostructures, and shell thickness allows for the precise control of the band alignment structures, excitons wave functions and their interactions with the local environments.^{3–6} Therefore, QD materials have numerous potential optical and optoelectronic applications,⁷ such as in microlasers,^{6,8} solid-state lighting,⁹ *in vivo* imaging,¹⁰ pH sensors,^{11,12} and electrical signal monitors.^{13,14}

In particular, semiconductor nanoparticles are always suggested as promising candidates for electric field (voltage)

sensing *via* the quantum-confined Stark effect (QCSE).^{14–19} QCSE devices based on a quantum well (QW) structure have been proven useful in optical modulation applications.^{20,21} Semiconductor QDs are analogous to QWs with a semiconductor-based quantum-confined structure. Narrow transition linewidths and large spectral shifts can result in QD-based optoelectronic devices with an even better performance.^{15,22} When an external electric field was applied to spherically symmetric QDs, isotropic QCSE independent of the direction of the field was shown, which was in stark contrast to that of noncentrosymmetrical nanomaterials.^{23–26} However, the charged carriers on or near the QD surface can induce a randomly oriented local electric field due to nonradiative Auger recombination (AR) or surface trap states.^{15,26–28} The random local field would lead to spectral broadening in the ensemble, due to which it is difficult for QDs to exhibit a measurable ensemble Stark effect. If the local field is eliminated, QCSE in QD ensembles can be readily observable at room temperature and also, the response of the absorbing state can be possibly characterized in the ensemble measurement. Thereby, this will promote the study of electroabsorption in quantum nanostructures because of their great promise in the advancement of electro-optic

^aAdvanced Photonics Center, Southeast University, Nanjing 210096, China. E-mail: jyzhang@seu.edu.cn

^bNational Laboratory of Solid State Microstructures, School of Physics, and Collaborative Innovation Center of Advanced Microstructures, Nanjing University, Nanjing 210093, China. E-mail: wxiaoyong@nju.edu.cn

†Electronic supplementary information (ESI) available. See DOI: 10.1039/c9nr03061a

modulation.^{17,24,29} Recently, phase-pure wurtzite (WZ) CdSe/CdS core/shell QDs have been proven to efficiently inhibit AR and the consequent photoluminescence (PL) blinking,^{6,10} which are closely related to the gradient alloy interface. Thus, this reveals more than 3 orders of magnitude increase in the biexciton Auger lifetime (from 67 ps to over 100 ns) for CdSe/CdS QDs with 19 CdS monolayers (19 MLs; 1 ML = 0.35 nm). Meanwhile, the epitaxial growth of the CdS shell and the nearly perfect alloyed interface can also sufficiently suppress the surface and interfacial defects^{5,6,10,30,31} while simultaneously acting as a barrier to prevent further field-driven ionization.¹⁵ Hence, the thick-shell WZ CdSe/CdS QDs can inhibit the random local field induced by nonradiative AR or defect states in favor of the study of their QCSE. Generally, it is suggested that PL blinking is derived from the charged exciton states in QDs through two main channels: multiexciton ionization and direct carrier trapping.^{32–34} However, the relationship between the PL blinking behavior and the ensemble Stark effect is still unclear in such a core/shell quantum-confined system.

In this work, we investigated QCSE for an ensemble of phase-pure WZ CdSe/CdS core/shell QDs. Our results showed that thick-shell CdSe/CdS QDs (11 MLs) exhibited a remarkable Stark effect in PL and absorption. The energy shifts in the emission and absorption peaks were found to be a typical quadratic function of the external field. On the other hand, it showed inconspicuous optical modulations in moderate-shell (5 MLs) and ultrathick-shell (15 MLs) QDs as compared to that in thick-shell QDs. According to the analysis of their time-dependent PL blinking behavior, the phenomenon was attributed to the impact of a large number of surface defect states and the strain-induced internal exciton trapping defects. At the same time, the field-dependent PL lifetime and exciton polarizability were also studied. Furthermore, the field-driven multiexciton process was explored in thick-shell CdSe/CdS QDs for the first time by amplified stimulated emission (ASE) measurements. Finally, these studies will enhance our knowledge of the Stark effect under the conditions of shell-thickness-dependent PL behaviors and will possibly contribute to the development of electro-optic modulators based on QD nanomaterials.

Experimental

Synthesis of phase-pure WZ CdSe/CdS core/shell QDs

Phase-pure WZ CdSe/CdS core/shell QDs were synthesized by the following two steps. First, the WZ CdSe cores were synthesized at 380 °C.¹⁰ Then, the CdS shell on the surface of the CdSe cores was epitaxially grown *via* the successive ionic layer adsorption and reaction (SILAR) method at a high temperature (310 °C).⁶

Device fabrication

The purified CdSe/CdS QDs in methylbenzene were added into a PMMA-methylbenzene solution (10 wt%); the volume fraction of the QDs in the polymer was less than 5%. Then, the

resulting QD solution was centrifuged at 4000 rpm for five minutes to remove possible aggregates. The SiO₂ dielectric layer (500 nm) was employed as an isolation medium between the ITO electrode (200 nm) and the QD polymeric film in order to avoid the effect of the electric current on the QCSE device. The SiO₂ layer was prepared by electron-beam deposition on the surface of the ITO electrode. The above QD solution was spin-coated onto the ITO/SiO₂ substrate and then quickly dried under vacuum. Finally, we obtained sandwich-like devices by attaching a second ITO electrode to each QD polymeric film using transparent glue. The exact distance between the two ITO electrodes was about 10 μm in the device (Fig. S1†). A direct current stabilized voltage source (PINTEK HA-800) was used to apply the external electric field oriented perpendicular to the sample surface.

Structural characterizations

Transmission electron microscopy (TEM) images were obtained on an FEI Tecnai G2 electron microscope. Three kinds of CdSe/CdS QDs have the same core diameter of 4.3 nm. The cross-section image of the QCSE device was measured by Carl Zeiss Ultra Plus field emission scanning electron microscopy (SEM).

Optical measurements

The absorption spectra were measured using a UV-Vis-NIR spectrophotometer (UV3600, Shimadzu). The PL emission spectra were collected with a fast optical multichannel analyzer (SpectraPro-300i, Acton Research Corporation). The excitation pulse was from an amplified femtosecond Ti:Sapphire laser system (800 nm, 1 kHz, 100 fs; Legend-F-1k, Coherent), and the 400 nm pump source was eventually obtained from a β-barium borate crystal. The PL decay traces were recorded using an electrically triggered streak camera system (C5680, Hamamatsu). For the blinking measurement, a picosecond supercontinuum fiber laser (490 nm, 4.9 MHz; NKT Photonics EXR-15) was employed as the excitation source. The PL emission from a single QD was collected with the confocal microscope and then sent to a single-photon counting system. The PL blinking traces of thirty QDs were randomly measured for each kind of QD. For the ASE measurement, a stripe pump was acquired using a cylindrical lens (10 cm focal length). The stripe modal confined pump pulses were perpendicular to the surface of the QCSE device. Then, the edge emitted beam was collected from the lateral parallel to the films by an optically triggered streak camera system. All measurements were conducted at room temperature.

Results and discussion

The phase-pure WZ CdSe/CdS core/shell QDs with 5, 11, and 15 ML CdS shells were synthesized using the SILAR method.⁶ In order to study the effect of an external electric field on the optical properties of QDs, we designed a multilayer device structure (Fig. 1a). The SiO₂ layer (500 nm) was first deposited

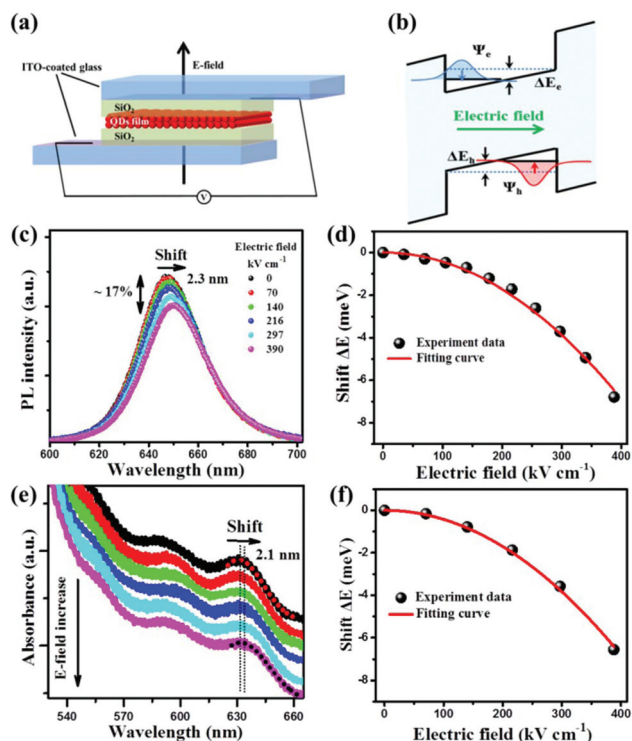


Fig. 1 (a) The structure of the QCSE device used for measuring optical properties of QDs under the electric field. (b) Schematic of the field-induced changes of band alignment and exciton localization in QD. (c) PL spectra of thick-shell CdSe/CdS QDs (11 MLs) in the QCSE device with increasing electric field strength. (d) The Stark shift *versus* electric field for the PL spectra in (c). The red line represents a fit to the shift as a quadratic function of the field. (e) Absorption spectra of thick-shell CdSe/CdS QDs under the electric field. The red and black dashed lines are the Gaussian fitting curves. The spectra are vertically shifted for clarity. (f) The Stark shift in the first excitonic absorption peak as a function of the electric field for the spectra in (e). The red line presents a fitting curve by a quadratic function of the electric field.

on the surface of a transparent indium tin oxide (ITO) electrode as an isolation layer. Semiconductor QDs were embedded in thin polymeric (methyl methacrylate) (PMMA) films (10 μm) by spin-coating a QDs-PMMA solution onto the above SiO_2 -coated ITO glass. Then, the second ITO electrode was attached to the QD film using glue, thus obtaining a sandwich-like ITO/ SiO_2 /QDs-PMMA/ SiO_2 /ITO structure. Fig. 1b shows the schematic of the field-induced changes in energy levels and exciton localization. The physical origin of QCSE was induced by the spatial separation of electron and hole wave functions with the electric field increase, followed by the buildup of an internal electric field (dipole) that opposed the external field.²¹ Importantly, this gave rise to distortion in the band alignment, thus resulting in a shift in the luminescence, a lowered probability of radiative recombination, and an increased lifetime.^{35–37}

For these devices, the PL and absorption properties from the photoexcited QCSE device were monitored following the changes in the external electric field. Fig. 1c shows the PL spectra of thick-shell CdSe/CdS QDs (11 MLs) with increasing

field strength, where the excitation wavelength is 400 nm. The PL spectra showed an obvious Stark shift in the peak position with a redshift of ~ 2.3 nm, and it was symmetric with the shift under the reverse electric field (Fig. S2[†]). The spectral shifts in the ensemble emission could be well-fitted by a purely quadratic function of the electric field (Fig. 1d). Therefore, this revealed that the Stark effect in the emitting state was characterized by the polarizable character and the absence of a significant permanent dipole moment. In this case, the average dipole moment may have reached zero with the distribution of dipole orientations relative to the external field. At the same time, the PL intensity showed remarkable quenching of $\sim 17\%$ and the PL spectra slightly broadened by $\sim 6\%$ (Fig. S3a[†]), as expected features of QCSE in semiconductor nanoparticles.^{37,38} Fig. 1e shows the absorption spectra of thick-shell CdSe/CdS QDs under different electric fields. On increasing the electric field strength, the redshift (~ 2.1 nm) in the first exciton absorption peak also exhibited quadratic dependence on the external electric field (Fig. 1f), indicating that the spectral shift was dominated by the quadratic Stark effect similar to the emitting state. Concomitant with the redshift in the absorption peak, $\sim 9\%$ decrease in the absorption intensity and $\sim 10\%$ increase in the full width at half-maximum were observed (Fig. S3b[†]). The results provide a possibility to efficiently tune the absorption properties by an external field, which is meaningful for the applications of QD-based QCSE in electroabsorption modulators.

However, the field-dependent optical properties in the moderate-shell (5 MLs) CdSe/CdS QDs showed nearly no spectral shifts, while the shifts for ultrathick-shell (15 MLs) CdSe/CdS QDs were not as obvious as that for the thick-shell QDs (Fig. S4[†]). The following time-dependent PL measurements at the single-particle level revealed that moderate-shell and ultrathick-shell QDs were likely to suffer from the local electric field. Fig. 2a–c present the TEM images of these three kinds of CdSe/CdS core/shell QDs. Fig. 2d–f show the time-dependent PL intensity traces of single CdSe/CdS QD with moderate, thick, and ultrathick CdS shells, respectively (for more samples, please see Fig. S5[†]). The PL intensity from an individual thick-shell CdSe/CdS QD (Fig. 2e) was continuously at the “On” state. This finding was in striking contrast to that for a moderate-shell QD (Fig. 2d), which displayed obvious PL blinking and intermittency periods (“Off” state). The blinking “Off” state could be induced by multiple charged excitons or the exciton trapping process, indicating that a large number of deep surface traps were possible in moderate-shell QDs.^{39–42} Hence, thick-shell CdSe/CdS QDs showed more high-efficiency suppression of the surface defect states than moderate-shell QDs. Nevertheless, when the CdS shell thickness increased towards 15 MLs (Fig. 2f), enhanced PL intensity fluctuations and an intermediate (“Int”) state were observed with a lower lifetime of 33 ns (blue region) with respect to the “On” state of 43 ns (red region) (Fig. S6[†]). The PL intensity fluctuations and the “Int” state may have been caused by more exciton-trapping defects^{43,44} at the interface and inside the ultrathick shells arising from the release of lattice strain with the further

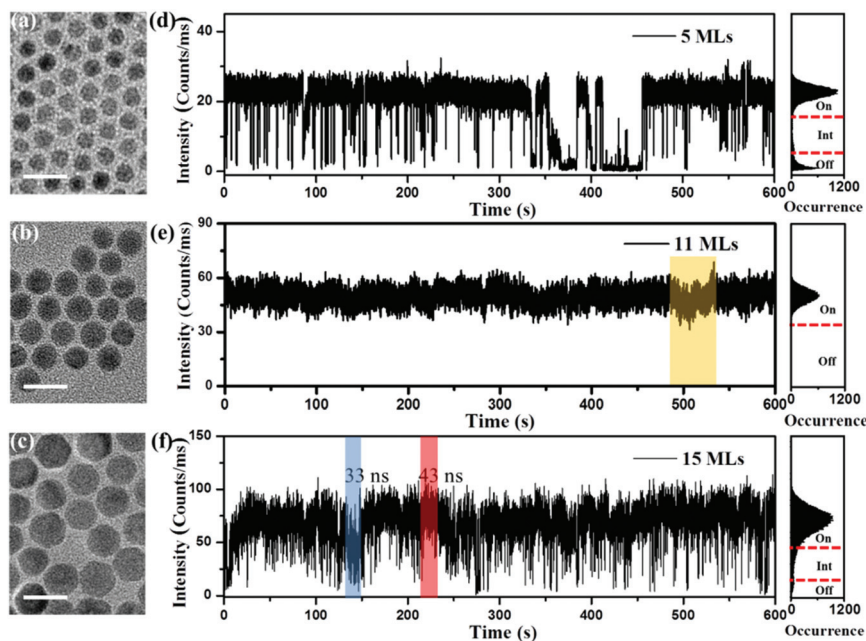


Fig. 2 (a–c) TEM images of phase-pure CdSe/CdS QDs with 5, 11, and 15 ML CdS shells, respectively. Scale bars are 20 nm. PL intensity traces of a single CdSe/CdS QD with different shell thicknesses: 5 MLs (d), 11 MLs (e), and 15 MLs (f). The measurements were performed with a time resolution of 10 ms. Histograms reveal the statistical distribution of the intensity in the trace. “On”, “Int”, and “Off” states are separated by the red dashed line.

growth of the CdS shell.^{6,44–46} The exciton-trapping defects also led to a charged state in QDs. Obviously, the strain-induced defect states barely formed in thick-shell CdSe/CdS QDs as compared to that in ultrathick-shell QDs. Besides, the PL QY measurements showed that the QYs of CdSe/CdS QDs rapidly increased from 75% (5 MLs) to 92% (11 MLs) on increasing the thickness of the CdS shell due to the improved surface passivation and suppression of nonradiative channels.^{5,6,10} However, with the further increase in shell thickness, QYs of the ultrathick QDs decreased to ~83%. This decrease in QYs indicated that the nonradiative process increased owing to the lattice strain-induced defects and more electron delocalization in the ultrathick shell.^{6,31,45–47} Therefore, the variation trend of shell-dependent QYs was consistent with the blinking behavior of CdSe/CdS QDs; they all exhibited a nonmonotonic behavior as a function of shell thickness. Therefore, a further study suggested that thick-shell CdSe/CdS QDs could minimize the adverse impact of the random local electric field induced by the charged exciton states, which is crucial for the observation of QCSE in QD ensembles.

Fig. 3 shows the typical PL decay traces of thick-shell CdSe/CdS QDs at the electric fields of 0 and 390 kV cm^{-1} . Despite significant changes in the PL and absorption properties, the PL lifetime did not show evident increase with the applied electric field, which was also observed in the report by Bozyigit *et al.*⁴⁷ The weakly field-dependent lifetime may be relative to the increased electron trapping in the shell regions due to the enhancement of carrier diffusion under an external field.^{31,47} The decreased PL intensity was affected by the reduction in

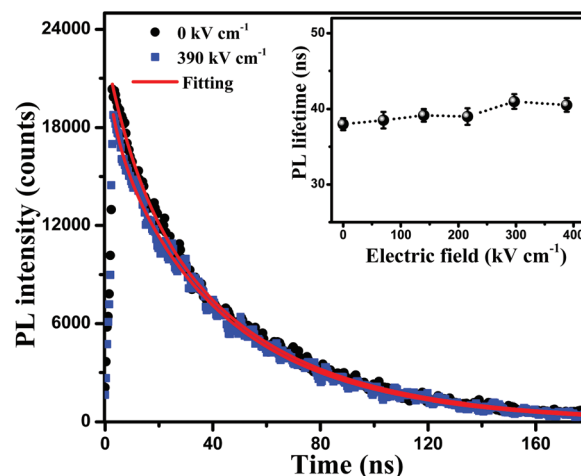


Fig. 3 PL decay traces of thick-shell CdSe/CdS QDs in QCSE device measured at the electric fields of 0 and 390 kV cm^{-1} , respectively. The red lines are fitting curves with bi-exponential function; the adjusted R^2 values are all larger than 0.99. Inset shows the PL lifetime as a function of the external electric field.

absorbance, as observed above, and by the dissociation of excitons by the force of the electric field. Importantly, the nearly field-independent PL lifetime and the related optical properties (spectral redshift and broadening as well as decreased emission intensity, Fig. S7a†) excluded the possibility of many nonradiative processes being the source of optical modulations. Thereby, this further confirmed that the charged state was indeed largely suppressed in most thick-shell CdSe/CdS

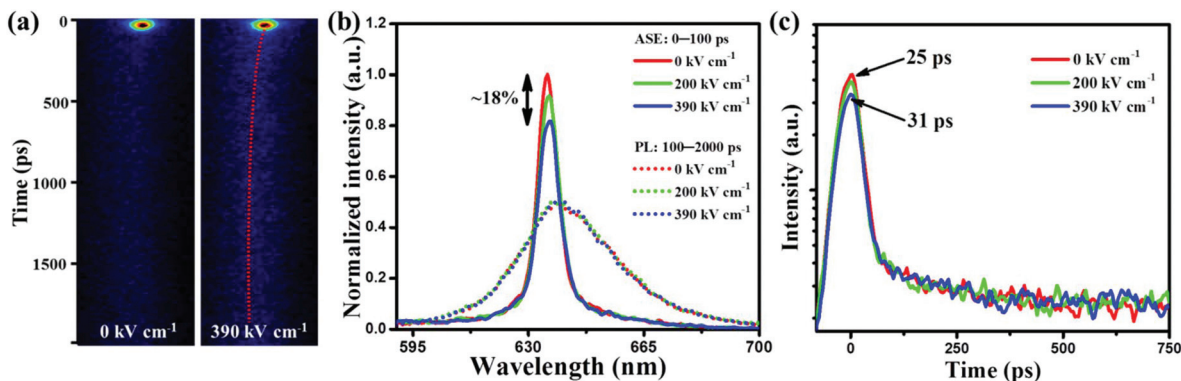


Fig. 4 (a) Time-resolved PL spectrogram of thick-shell CdSe/CdS QDs in a QCSE device for 0 and 390 kV cm^{-1} under a stripe femtosecond-pulsed excitation at 400 nm. The red dashed line presents the variation trend of the emission peak position. (b) ASE and PL spectra as a function of the electric field extracted from the spectrogram (a) with integrated time ranges of 0–100 ps and 100–2000 ps, respectively. (c) The ASE decay traces of thick-shell CdSe/CdS QDs under different electric fields.

QDs, due to which they could realize more distinct QCSE in comparison to moderate-shell and ultrathick-shell QDs.

Here, we used the quadratic energy-field expression to estimate the exciton polarizability (α) of thick-shell QDs.¹⁵ The α values were found to be $\sim 8.6 \times 10^{-5}$ and $\sim 8.4 \times 10^{-5}$ $\text{meV cm}^2 \text{ kV}^{-2}$ by fitting the experimental results in Fig. 1d and f, respectively. Moreover, the theoretical polarizability of the excitons in thick-shell QDs was estimated to be around $\sim 1.5 \times 10^{-4}$ $\text{meV cm}^2 \text{ kV}^{-2}$ by an effective core radius of 3.2 nm,⁴⁸ as calculated using the wavelength of the first excitonic absorption peak (632 nm).⁴⁹ The α value measured for thick-shell QD ensembles was smaller than the corresponding calculated result, implying that the field modulation effect may be weakened by a few probable radiative traps near the band edge.⁵⁰ This also coincided with some slight intensity fluctuations (orange region) in the PL intensity trace, as shown in Fig. 2e.

The above results demonstrated that the defect states on the surface and inside QDs seriously restrained their ensemble QCSE, while the presence of very few trap states in some thick-shell QDs did not matter much for the ensemble measurement. For further insights into the trap states in the field-driven exciton process, we measured the ASE performance of thick-shell CdSe/CdS QDs under different electric fields. Fig. 4a displays the time-resolved PL spectrogram of field-effect CdSe/CdS QDs for 0 and 390 kV cm^{-1} applied fields. As shown in Fig. 4b, fast ASE (0–100 ps) exhibits clear decrease of 18% in the emission intensities on increasing the field strength. The decreased emission efficiency of multiexcitons could be associated with the field-enhanced electron delocalization in thicker shell QDs.⁴⁷ However, because of the repulsive Coulomb interaction among the excitons (Fig. S7b†)⁵¹ and the internal screen effect of the multiexciton state for the external field, the field-induced shift (~ 0.6 nm) of the ASE peak was inconspicuous. The corresponding evolution of ASE decay dynamics is illustrated in Fig. 4c. When the electric field progressively strengthened, the ultrafast lifetime of ASE increased from 25 to 31 ps, which showed stronger dependence on the

field than on a single exciton state. In addition, when all multiexcitons decayed (>100 ps), the remaining single exciton gradually relaxed from the multiexciton-induced higher energy state to a band-edge emitting state due to the decrease in repulsive Coulomb interactions. Therefore, the PL spectra present a continuous redshift along with decay time (Fig. S7c†); the variation trend of the corresponding emission peak position is shown as a red dashed line in Fig. 4a. Meanwhile, the enhancement in electron delocalization and the repulsive exciton–exciton interactions in the multiexciton process could promote the diffusion of electron wave functions into the CdS shells, which increased the trapping probability of the electrons on the surface and within the thick-shell regions.^{5,31,52} Therefore, as shown in Fig. 4b, the long-lived delay component (100–2000 ps) exhibits nearly field-independent PL emission spectra, indicating that the dynamic relaxation process and the potential electron trapping can weaken the Stark effect of a single exciton.

Conclusions

In summary, QCSE in the ensemble of phase-pure thick-shell CdSe/CdS QDs was systematically studied under an external electric field. We observed a pronounced redshift and broadening of PL and absorption spectra as well as decrease in the intensity. On this basis, we studied the relationship between the shell-thickness-dependent PL blinking behavior and the Stark effect by the analysis of time-dependent PL intensity measurements. The results showed that thick-shell CdSe/CdS QDs could provide effective suppression of the local electric field in comparison to moderate-shell and ultrathick-shell QDs, thus favoring the realization of ensemble QCSE. Besides, deeper insights into the properties of field-driven multiexciton emissions indicated that fast ASE showed decrease of 18% in the emission intensities and an evident field-dependent decay process. However, the smaller exciton polarizability suggested

that a few traps still existed in some thick-shell QDs. In order to reduce such trap states and eliminate their adverse effect on QCSE as far as possible, more improvements are needed in future works to synthesize thick-shell QDs with a wider graded interface and smoother confinement potential. Finally, these optical properties (changes in emission and absorption intensities and spectral shifts) in QCSE devices open the potential possibility of field-sensitive QDs to achieve electro-optic sensing.

Conflicts of interest

There are no conflicts to declare.

Acknowledgements

We thank Prof. E. Feddi, his PhD student, N. Aghoutane, and Prof. F. Dujardin for their useful discussion on exciton polarizability. This work was supported by the National Basic Research Program of China (973 Program, 2015CB352002), the Postgraduate Research & Practice Innovation Program of Jiangsu Province (KYCX17_0064), the Fundamental Research Funds for the Central Universities (2242017K41009 and 2242018K41021), and the Science and Technology Support Program of Jiangsu Province (BE2018117 and BE2016021).

References

- C. B. Murray, D. J. Norris and M. G. Bawendi, *J. Am. Chem. Soc.*, 1993, **115**, 8706–8715.
- B. K. Chen, N. Pradhan and H. Z. Zhong, *J. Phys. Chem. Lett.*, 2018, **9**, 435–445.
- X. Peng, L. Manna, W. Yang, J. Wickham, E. Scher, A. Kadavanich and A. P. Alivisatos, *Nature*, 2000, **404**, 59–61.
- P. Reiss, M. Protière and L. Li, *Small*, 2009, **5**, 154–168.
- S. Christodoulou, G. Vaccaro, V. Pinchetti, F. De Donato, J. Q. Grim, A. Casu, A. Genovese, G. Vicidomini, A. Diaspro, S. Brovelli, L. Manna and I. Moreels, *J. Mater. Chem. C*, 2014, **2**, 3439–3447.
- C. Liao, R. Xu, Y. Xu, C. Zhang, M. Xiao, L. Zhang, C. Lu, Y. Cui and J. Zhang, *J. Phys. Chem. Lett.*, 2016, **7**, 4968–4976.
- J. M. Pietryga, Y. S. Park, J. Lim, A. F. Fidler, W. K. Bae, S. Brovelli and V. I. Klimov, *Chem. Rev.*, 2016, **116**, 10513–10622.
- M. Saliba, S. M. Wood, J. B. Patel, P. K. Nayak, J. Huang, J. A. Alexander-Webber, B. Wenger, S. D. Stranks, M. T. Hörlantner, J. T. W. Wang, R. J. Nicholas, L. M. Herz, M. B. Johnston, S. M. Morris, H. J. Snaith and M. K. Riede, *Adv. Mater.*, 2016, **28**, 923–929.
- X. Dai, Z. Zhang, Y. Jin, Y. Niu, H. Cao, X. Liang, L. Chen, J. Wang and X. Peng, *Nature*, 2014, **515**, 96–99.
- O. Chen, J. Zhao, V. P. Chauhan, J. Cui, C. Wong, D. K. Harris, H. Wei, H.-S. Han, D. Fukumura, R. K. Jain and M. G. Bawendi, *Nat. Mater.*, 2013, **12**, 445–451.
- I. L. Medintz, M. H. Stewart, S. A. Trammell, K. Susumu, J. B. Delehanty, B. C. Mei, J. S. Melinger, J. B. Blanco-Canosa, P. E. Dawson and H. Mattoussi, *Nat. Mater.*, 2010, **9**, 676–684.
- F. Bruni, J. Pedrini, C. Bossio, B. Santiago-Gonzalez, F. Meinardi, W. K. Bae, V. I. Klimov, G. Lanzani and S. Brovelli, *Adv. Funct. Mater.*, 2017, **27**, 1605533.
- A. L. Efros, J. B. Delehanty, A. L. Huston, I. L. Medintz, M. Barbic and T. D. Harris, *Nat. Nanotechnol.*, 2018, **13**, 278–288.
- K. Park, Z. Deutsch, J. J. Li, D. Oron and S. Weiss, *ACS Nano*, 2012, **6**, 10013–10023.
- S. Empedocles and M. Bawendi, *Science*, 1997, **278**, 2114–2117.
- Y. Kuo, J. Li, X. Michalet, A. Chizhik, N. Meir, O. Bar-Elli, E. Chan, D. Oron, J. Enderlein and S. Weiss, *ACS Photonics*, 2018, **5**, 4788–4800.
- A. W. Achtstein, A. V. Prudnikau, M. V. Ermolenko, L. I. Gurinovich, S. V. Gaponenko, U. Woggon, A. V. Baranov, M. Y. Leonov, I. D. Rukhlenko, A. V. Fedorov and M. V. Artemyev, *ACS Nano*, 2014, **8**, 7678–7686.
- O. B. Elli, D. Steinitz, G. Yang, R. Tenne, A. Ludwig, Y. Kuo, A. Triller, S. Weiss and D. Oron, *ACS Photonics*, 2018, **5**, 2860–2867.
- J. D. Marshall and M. J. Schnitzer, *ACS Nano*, 2013, **7**, 4601–4609.
- Y.-H. Kuo, Y. K. Lee, Y. Ge, S. Ren, J. E. Roth, T. I. Kamins, D. A. B. Miller and J. S. Harris, *Nature*, 2005, **437**, 1334–1336.
- D. A. B. Miller, D. S. Chemla, T. C. Damen, A. C. Gossard, W. Wiegmann, T. H. Wood and C. A. Burrus, *Phys. Rev. Lett.*, 1984, **53**, 2173–2176.
- S. A. Empedocles, D. J. Norris and M. G. Bawendi, *Phys. Rev. Lett.*, 1996, **77**, 3873–3876.
- J. Müller, J. M. Lupton, P. G. Lagoudakis, F. Schindler, R. Koeppel, A. L. Rogach, J. Feldmann, D. V. Talapin and H. Weller, *Nano Lett.*, 2005, **5**, 2044–2049.
- N. V. Tepliakov, I. O. Ponomareva, M. Y. Leonov, A. V. Baranov, A. V. Fedorov and I. D. Rukhlenko, *J. Phys. Chem. C*, 2016, **120**, 2379–2385.
- N. N. Hewa-Kasakarage, M. Kirsanova, A. Nemchinov, N. Schmall, P. Z. El-Khoury, A. N. Tarnovsky and M. Zamkov, *J. Am. Chem. Soc.*, 2009, **131**, 1328–1334.
- J. Müller, J. M. Lupton, A. L. Rogach, J. Feldmann, D. V. Talapin and H. Weller, *Phys. Rev. B: Condens. Matter*, 2005, **72**, 205339.
- S. A. Empedocles and M. G. Bawendi, *J. Phys. Chem. B*, 1999, **103**, 1826–1830.
- H. D. Robinson and B. B. Goldberg, *Phys. Rev. B: Condens. Matter Mater. Phys.*, 2000, **61**, R5086–R5089.
- N. V. Tepliakov, M. Y. Leonov, A. V. Baranov, A. V. Fedorov and I. D. Rukhlenko, *Opt. Express*, 2016, **24**, A52–A57.

- 30 L. Zhang, C. Liao, B. Lv, X. Wang, M. Xiao, R. Xu, Y. Yuan, C. Lu, Y. Cui and J. Zhang, *ACS Appl. Mater. Interfaces*, 2017, **9**, 13293–13303.
- 31 L. Zhang, H. Li, C. Liao, H. Yang, R. Xu, X. Jiang, M. Xiao, C. Lu, Y. Cui and J. Zhang, *J. Phys. Chem. C*, 2018, **122**, 25059–25066.
- 32 F. Hu, C. Yin, H. Zhang, C. Sun, W. W. Yu, C. Zhang, X. Wang, Y. Zhang and M. Xiao, *Nano Lett.*, 2016, **16**, 6425–6430.
- 33 A. L. Efros and M. Rosen, *Phys. Rev. Lett.*, 1997, **78**, 1110–1113.
- 34 L. A. Padilha, I. Robel, D. C. Lee, P. Nagpal, J. M. Pietryga and V. I. Klimov, *ACS Nano*, 2011, **5**, 5045–5055.
- 35 G. W. Wen, J. Y. Lin, H. X. Jiang and Z. Chen, *Phys. Rev. B: Condens. Matter*, 1995, **52**, 5913–5922.
- 36 R. Korlacki, R. F. Saraf and S. Ducharme, *Appl. Phys. Lett.*, 2011, **99**, 153112.
- 37 J. Seufert, M. Obert, M. Scheibner, N. A. Gippius, G. Bacher, A. Forchel, T. Passow, K. Leonardi and D. Hommel, *Appl. Phys. Lett.*, 2001, **79**, 1033–1035.
- 38 R. M. Kraus, P. G. Lagoudakis, A. L. Rogach, D. V. Talapin, H. Weller, J. M. Lupton and J. Feldmann, *Phys. Rev. Lett.*, 2007, **98**, 017401.
- 39 C. Galland, Y. Ghosh, A. Steinbruck, M. Sykora, J. A. Hollingsworth, V. I. Klimov and H. Htoon, *Nature*, 2011, **479**, 203–207.
- 40 J. Zhao, G. Nair, B. R. Fisher and M. G. Bawendi, *Phys. Rev. Lett.*, 2010, **104**, 157403.
- 41 D. E. Gómez, J. van Embden, P. Mulvaney and M. J. Fernée, *ACS Nano*, 2009, **8**, 2281–2287.
- 42 P. A. Frantsuzov and R. A. Marcus, *Phys. Rev. B: Condens. Matter Mater. Phys.*, 2005, **72**, 155321.
- 43 S. Seth, T. Ahmed and A. Samanta, *J. Phys. Chem. Lett.*, 2018, **9**, 7007–7014.
- 44 B. Omogo, F. Gao, P. Bajwa, M. Kaneko and C. D. Heyes, *ACS Nano*, 2016, **10**, 4072–4082.
- 45 X. Chen, Y. Lou, A. C. Samia and C. Burda, *Nano Lett.*, 2003, **3**, 799–803.
- 46 G. A. Beane, K. Gong and D. F. Kelley, *ACS Nano*, 2016, **10**, 3755–3765.
- 47 D. Bozyigit, O. Yarema and V. Wood, *Adv. Funct. Mater.*, 2013, **23**, 3024–3029.
- 48 S. Wu and W. Xia, *J. Appl. Phys.*, 2013, **114**, 043709.
- 49 W. W. Yu, L. Qu, W. Guo and X. Peng, *Chem. Mater.*, 2003, **15**, 2854–2860.
- 50 J. M. Zhang, X. K. Zhang and J. Y. Zhang, *J. Phys. Chem. C*, 2009, **113**, 9512–9515.
- 51 A. F. Cihan, Y. Kelestemur, B. Guzelurk, O. Yerli, U. Kurum, H. G. Yaglioglu, A. Elmali and H. V. Demir, *J. Phys. Chem. Lett.*, 2013, **4**, 4146–4152.
- 52 D. A. Hanifi, N. D. Bronstein, B. A. Koscher, Z. Nett, J. K. Swabeck, K. Takano, A. M. Schwartzberg, L. Maserati, K. Vandewal, Y. Burt, A. Salleo and A. P. Alivisatos, *Science*, 2019, **363**, 1199–1202.